Republic of Iraq
Ministry of Higher Education & Scientific Research
University of Diyala - College of Science Department of Physics

Efficiency Enhancement of Porous Silicon Solar Cell by Embedding of Some Metal Oxides Nanoparticles

A Thesis

Submitted to the Council of College of Science University of Diyala in Partial Fulfillment of the Requirements for the Degree of Doctor of Philosophy in Physics

By

Shahlaa Mundher Abd Al-Hussan

B.Sc. in Physics, 2012

M.Sc. in Physics, 2016

Supervised By

Prof. Dr.
Nabeel Ali Bakr

Prof. Dr.
Ahmed Naji Abd

2021 A.D.

1442 A.H

هُوَ الَّذِي جَعَلَ الشَّمْسَ ضِيَاءً وَالْقَمَرَ نُورًا
وَقَدَّرَهُ مَنَازِلَ لِتَعْلَمُوا عَدَدَ السِّنِينَ
وَالْحِسَابَ مَا خَلَقَ اللَّهُ ذَلِكَ إِلَّا بِالْحَقِّ
يُفَصِّلُ الْآيَاتِ لِقَوْمٍ يَعْلَمُونَ ﴿5﴾

صدق الله العظيم

سورة يونس : الآية -5-

Dedications

To the sun of truth to Allah reward. (The owner of the age and time)

(Aba Saleh Al- Mahdi)

To the first teacher who gave me the strength and patience and diligence.

(My father)

To my way candle that lit up my life and stayed up nights to my care.

my love ***(My dear Mother)***

To those have stood beside me and sacrificed for me.

(Avuncular Abdulla H. Aljubori *and* ***My Brothers)***

To the head of Diyala Environment

(legal counsel (Abdalla Hadi Al-shamary)) to his help.

Shahlaa M. Al-Shamary

Acknowledgments

First of all, I would like to thank ***ALLAH*** for his generosity and mercy in giving the strength and the ability to complete my studies.

I would like to express my deep gratitude and appreciation to my supervisors ***Prof. Dr. Nabeel Ali Bakr*** (Department of Physics, College of Science, University of Diyala) and ***Prof. Dr. Ahmed Naje Abd*** (Department of Physics, College of Science, Al-Mustansirya University) for suggesting the topic of the thesis, their continuous advice and their guidance throughout this work.

I would like to express my profound gratitude to ***prof. Dr. Ziad Tariq Khodair*** for his kind cooperation and constant support and ***Prof. Dr. Sabah Anwer Salman***, for his constant encouragement throughout my studies, (Department of Physics, College of Science, University of Diyala).

Finally, Special thanks to the Dean of the College of Science, University of Diyala ***Prof. Dr. Tahseen H. Mubarak*** and all the Staff of the Department of Physics for their assistance.

Shahlaa M. Al-Shamary

Supervisor Certification

We certify that this thesis entitled **"Efficiency Enhancement of Porous Silicon Solar Cell by Embedding of Some Metal Oxides Nanoparticles"** submitted by (***Shahlaa Mundher Abd Al-Hussan***) was prepared under our supervision at the Department of Physics, College of Science, University of Diyala and Department of Physics, College of Science, Al-Mustansirya University, in a partial fulfillment of the requirements needed to award the Degree of Doctor of Philosophy (Ph. D.) of Science in Physics.

Signature:
Name: Dr. Nabeel A. Bakr
Title: Professor
Address: University of Diyala
Date: / / 2021

Signature:
Name: Dr. Ahmed N. Abd
Title: Professor
Address: Al-Mustansiriya University
Date: / / 2021

Head of the Physics Department

In view of the available recommendations, I forward this thesis for debate by the examination committee.

Signature:
Name: Dr. Ammar A. Habeeb
Title: Assistant Professor
Address: Head of the physic department,
College of Science,
University of Diyala
Date: / / 2021

Linguistic Amendment

I certify that the thesis entitled **"Efficiency Enhancement of Porous Silicon Solar Cell by Embedding of Some Metal Oxides Nanoparticles"** presented by (***Shahlaa Mundher Abd Al-Hussan***) has been corrected linguistically, therefore, it is suitable for debate by examining committee.

Signature:

Name: **Dr. Karim H. Hassan**

Title: **Professor**

Address: **University of Diyala, College of science/ Department of Chemical**

Date: / / **2021**

Scientific Amendment

I certify that the thesis entitled **"Efficiency Enhancement of Porous Silicon Solar Cell by Embedding of Some Metal Oxides Nanoparticles"** presented by (***Shahlaa Mundher Abd Al-Hussan***) has been evaluated scientifically, therefore, it is suitable for debate by examining committee.

Signature:

Name: **Dr. Sabah I. Abbas**

Title: **Assistant Professor**

Address: **college of Science, Al- Karkh University**

Date: **/ / 2021**

Scientific Amendment

I certify that the thesis entitled **"Efficiency Enhancement of Porous Silicon Solar Cell by Embedding of Some Metal Oxides Nanoparticles"** presented by (***Shahlaa Mundher Abd Al-Hussan***) has been evaluated scientifically, therefore, it is suitable for debate by examining committee.

Signature:

Name: **Dr. Farouk I. Hussein**

Title: **Assistant Professor**

Address: **University of Baghdad, College of education for pure science**

Date: **/ / 2021**

Examination Committee Certificate

We certify that we have read this thesis entitled ***"Efficiency Enhancement of Porous Silicon Solar Cell by Embedding of Some Metal Oxides Nanoparticles"*** presented by ***(Shahlaa Mundher Abd Al-Hussan)*** and as an examine committee, we examined the student on its contents, and in what is related to it, and that in our opinion it meets the standard of a thesis for the ***Degree of Doctor of Philosophy (Ph.D.) in physics Science.***

Signature:
Name: **Dr. Sabah A. Salman**
Title: **Professor**
Date: / / **2021**
(Chairman)

Signature:
Name: **Dr. Ziad T. khodair**
Title: **Professor**
Date: / / **2021**
(Member)

Signature:
Name: **Dr. Ramiz A. Mohammed**
Title: **Professor**
Date: / / **2021**
(Member)

Signature:
Name: **Dr. Jasim M. Mansoor**
Title: **Assistant Professor**
Date: / / **2021**
(Member)

Signature:
Name: **Dr. Mushtak A. Jabbar**
Title: **Assistant Professor**
Date: / / **2021**
(Member)

Signature:
Name: **Dr. Nabeel A. Bakr**
Title: **Professor**
Date: / / **2021**
(Supervisor)

Signature:
Name: **Dr. Ahmed N. Abd**
Title: **Professor**
Date: / / **2021**
(Supervisor)

Approved by the Council of the College of Science:

Signature:
Name: **Dr. Tahseen H. Mubarak**
Title: **Professor**
Address: **Dean of College of the Science, University of Diyala**
Date: / / **2021**

Abstract

In this study, firstly electrochemical etching of the (n and p) type silicon wafers are used to prepare of (n and p) type of porous silicon with a current density of 10 $mA.cm^{-2}$ at 10 minutes. The structural and morphological of the PSi were studied by using XRD, AFM, FESEM, and FTIR spectroscopy. The XRD results showed that the (n and p) type of PSi are monocrystalline structure with strong, sharp, and narrow single peak, and preferred orientation along (400) plane. AFM has been used to investigate the Average grain size, porosity for porous silicon. Surface morphology of the (n and p) PSi layer are so smooth and homogeneous, and the film consists of matrix of random distribution nanocrystalline silicon pillars which have the same direction. FESEM has been used to study porous silicon layer surface morphology, while FTIR analysis showed that Si dangling bonds of the as-prepared PSi layer having large amount of hydrogen to form weak Si–H bonds.

Zinc oxide and lithium oxide nanoparticles are prepared separately by chemical precipitation and simple precipitation methods, respectively and deposited on silicon, FTO, and glass substrates by drop casting method to prepare thin films ZnO (Z_3) and Li_2O (L_1). Moreover, the structural, morphological and optical properties of the films were studied by using XRD, AFM, SEM, and (UV-Visble) spectrophotometer, respectively. The XRD results showed that the ZnO and Li_2O films are polycrystalline with hexagonal wurtzite structure and cubic structure, and preferred orientation along (101) and (003) planes, respectively. The crystallite size was measured using Scherrer's formula, and it was found that ZnO (Z_3) and Li_2O (L_1) thin films have a crystallite size of 22.04 and 45.6 nm respectively. AFM results showed homogenous and smooth thin films. Surface topography of the prepared thin films is studied by SEM. The results of UV-Vis spectra showed that all films have a good absorbance in Visible and near IR region. Consequently, it was chosen as an active absorption layer in applications of solar cell. The optical energy gap for allowed direct electronic transition was calculated using Tauc's

model and it was found that the values of energy gap of the films are 4.90 eV and 5.5 eV, respectively.

Finally, certain proportions (0.25:0.75), (0.5:0.5), and (0.75:0.25) of ($ZnO:Li_2O$) were mixed and deposited on porous silicon using drop casting method at thickness of 1.4 μm, then (Al) was deposited as a conductive electrode on the back face of the silicon cell by using thermal evaporation technology. After that, the characteristics of the solar cell and photodetector were investigated. The photocurrent density-voltage (J-V) curves characteristics of fabricated solar cells have been measured under simulated solar light (10 mW/m^2), and the parameters including V_{OC}, J_{SC}, FF% and η% of solar cells were calculated. The results showed that the solar cell fabricated of mixing ZnO (Z_3) with Li_2O (L_1) nanoparticles played a major role in increasing the solar cell's performance. The highest efficiency was obtained at mixing ratio (0.5: 0.5) for (ZnO: Li_2O) and its value was (11.09%) for heterojunction ($ZnO:Li_2O$)/PSi/p-Si/Al, and multi-junction based on (FTO/ZnO/Li_2O/PSi/p-Si/Al) layer as an active layer recorded higher efficiency of (24%) compared to the other fabricated solar cells. The spectral responsivety measurements for the prepared photodetectors showed that they worked within the range (350-1000) nm, the highest spectral responsivety value for heterojunctions ZnO/PSi/p-Si/Al can be used for photodetector applications within near-infrared and visible spectrum, where the spectral responsivity (R_λ) and specific detectivity (D*) of ZnO/PSi/p-Si/Al photodetectors are about (2.08A/W) and ($2.9x10^{13}$cm $Hz^{1/2}W^{-1}$) respectively, at λ~ 450 nm.

Table of Contents

List of Abbreviations

Abbreviation	*Definition*
AFM	Atomic Force Microscope
ASTM	American Society of Testing Materials
CB	Conduction Band
CPU	Central process unit
c-Si	Crystalline Silicon
DOS	Density Of State
ECE	Electrochemical etching
ETL	Electron Transport Layer
FESEM	Field Emission Scanning Electron Microscopy
FTIR	Fourier Transform-Infrared Spectroscopy
FTO	Fluorine−doped Tin Oxide
FWHM	Full Width at Half Maximum
GaAs	Gallium Arsenide
GaInAs	Gallium Indium Arsenide
GaInP	Gallium Indium Phosphate
hkl	Miller Indices
ICDD	International Center of Diffraction Data
IR	Infrared
I-V	Current-Voltage
J-V	Current density–Voltage
LIB	Lithium Ion Batteries

MCT	Minority Carrie Life Time
MJISCs	Multijunction Inverted solar cells
MPP	Maximum Power Point
NPs	Nanoparticles
NWs	Nanowires
OCVD	Open Circuit Voltage Decay
OP	Optical microscope
P	Porosity
PCE	Power Conversion Efficiency
PD	Photodetector
PECE	photo Electrochemical etching
PL	Photoluminescence
PSi	Porous Silicon
PSLs	Porous Silicon Layers
PV	Photovoltaic
QCE	Quantum Confinement Effect
RMS	Root Mean Square
R_s	Series resistance
R_{Sh}	Shunt resistance
SEM	Scanning Electron Microscope
Si Ns	Silicon Nanostructure
SOI	silicon-on-insulator
TCO	Transparent Conduction
TFSC	Thin Film Solar Cell

TSCs	Tandem Solar Cells
UHV	Ultrahigh Vacuum
UV	Ultra violet
VB_1	Initial Valence Band
VB_2	Second Valence Band
VB_3	Third Valence Band
Vis	Visible
V_{oc}	Open Circuit Voltage
W-H	Williamson-Hall
XRD	X- ray Diffraction

List of Symbols

Symbol	*Meaning*	*Units*
A	Absorbance	-
a,b* and *c	Lattice constants	Å
B	Constant	-
c	Speed of light	m/s
D	crystallite size	nm
$\mathbf{d_{hkl}}$	Inter planar spacing	Å
$\mathbf{D_{\lambda}^{*}}$	Spectral Detectivity	$\mathbf{cm.\ Hz^{1/2}.W^{-1}}$
E	Energy of photon	eV
$\mathbf{e^{-}}$	Electron	-
$\mathbf{E_a}$	Activated Energy	**eV**
$\mathbf{E_c}$	Bottom of Conduction Band	**eV**
$\mathbf{E_f}$	Fermi Energy Level	**eV**
$\mathbf{E_g}$	Optical Energy Gap	eV
$\mathbf{E_{Redox}}$	Reduction Potential	eV
$\mathbf{E_v}$	Top of Valence Band	**eV**
F.F	Filling Factor	-
h	Planck 's constant	J.s
$\mathbf{h^{+}}$	Hole	-
hkl	Miller indices	-

hv	Photon energy	J
I	Incident light intensity	mW/cm^2
I_D	Diode current	mA
I_d	Dark current	mA
I_E	Electric current	mA
I_L	Light induced current	mA
I_{max}	Maximum current	mA
I_o	The saturation current density	mA
I_{ph}	The light-generated current density	mA
I_{SC}	Short circuit current	mA
I_{Sh}	Shunt current	mA
I_T	Transmitted light intensity	mW/cm^2
J_{max}	Current density at maximum power point	mA/cm^2
J_{SC}	Short−circuit current density	mA/cm^2
k	Shape factor	-
K_B	Boltzmann constant	J/K
ǹ	The diode ideality factor	-
η	Efficiency	-
P_{in}	The incident power	mW/cm^2
P_{max}	Maximum power	mW/cm^2
q	The electron charge	-
r	The exponent	-
R_λ	Responsivity	$A.W^{-1}$

T	The temperature	K
T	Transmittance	-
t	Time	**S**
$\mathbf{T_r}$	Transmission	**%**
$\mathbf{t_t}$	Film Thickness	**nm**
V	Voltage	V
$\mathbf{V_a}$	Applied Voltage	**V**
$\mathbf{V_{max}}$	Maximum voltage	V
$\mathbf{V_{OC}}$	Open-circuit voltage	V
$\boldsymbol{\alpha}$	Optical absorption coefficient	cm^{-1}
$\boldsymbol{\lambda}$	The wavelength of the incident X-ray	nm
$\boldsymbol{n}$	Integer number	-
$\boldsymbol{\mathcal{A}}$	The active surface area of the cell	cm^2
$\boldsymbol{\theta}$	Bragg's angle	degree
$\boldsymbol{\beta}$	Full width at half maximum	Degree

List of Figures

List of Tables

Chapter One

Introduction

1.1 Introduction

Nanotechnology encompasses the creation and utilization of materials, devices and systems at the level of atoms and molecules. At nano-wavelength scales new physical properties emerge in these materials and new techniques are required to make them. Size constraints often produce qualitatively new behavior in nano – materials. Nanoscale researches on the optical, electronic properties of semiconductors at the nano-scale are experiencing astonishing growth [1].

Nanocrystals (NCs) are clumps of atoms that form a cluster. They are in order of molecules (~ 10 nm in diameter), but not as big as bulk matter. Although nanocrystals physical and chemical characteristics change, one of their big advantages over larger materials is that their size and surface can be precisely controlled and properties tuned [2].

Semiconductor nanocrystals show unique size-or shape-dependent optical properties due to the quantum confinement effects, thus it may find a wide range of applications in optoelectronic devices, photocatalysis, solar energy conversion and biological imaging and labeling [3-5]. For various aims of applications, the optical properties of semiconductor nanocrystals are required to be controllable. The tunability of optical properties of semiconductor nanocrystals have a key importance and would be beneficial to their applicability [6]. Over the last few years, advances in solid state physics have been characterized by a change from bulk crystal to a very small at least one of their three dimensions. Semiconductor nanocrystals are the subject of a rapidly developing field. It can be defined as crystals with dimensions ranging from (1-100) nm; above this size, they are termed microcrystals. These small-sized structures have at least one dimension in the nanoscale (<100 nm) and can be categorized according to their dimensionality as zero-dimensional (0D), one-dimensional (1D), two-dimensional (2D), and three-dimensional (3D) materials, as shown in

figure((1.1)(a)–(d)) [7]. The material can be classified depending on the dimension as listed in table (1.1).

Table (1.1): Classification of nanomaterial with regard to dimension [8].

Dimension	Example
0dimension <100 nm	Nanoparticles , quantum dots
1 dimension <100 nm	Nanotubes , Nanowire , Nanorods
2 dimensions <100 nm	Thin films, Coatings , Multilayer's
3 dimensions <100 nm	Nanometer-sized cluster

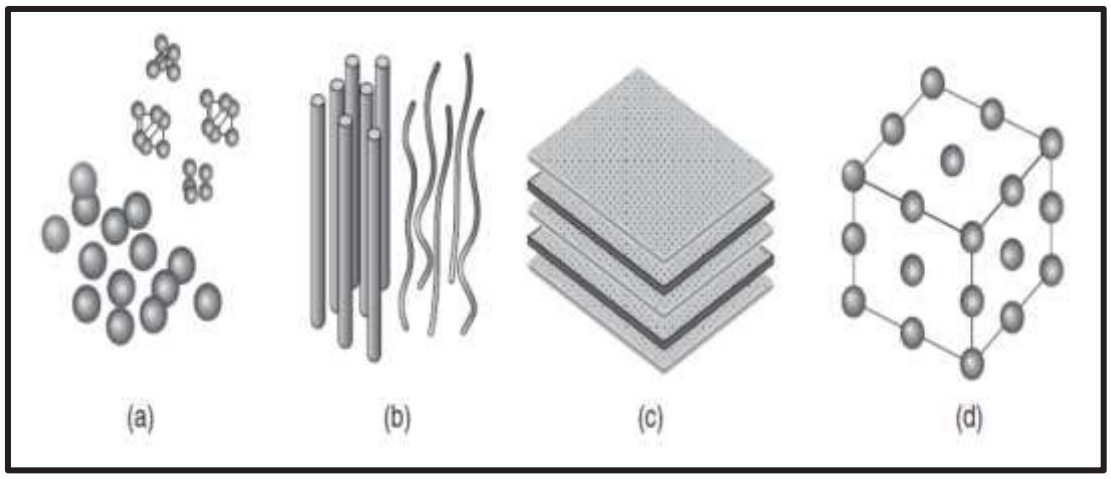

Fig.(1.1): Dimensional classification of nanomaterials: **(a):** 0D with all dimensions in the three directions are in the nanoscale ($\leq 10^{-9}$ m). Examples of this kind are nanoparticles, quantum dots, and clusters, **(b):** 1D where one dimension of the nanostructure will be outside the nanometer range. Nanorods, nanotubes, and nanofibers are included in this classification, **(c):** 2D with two dimensions outside the nanometer range. These include different types of thin films and plates, **(d):** 3Dwith all dimensions outside the nanoscale. Bulk amorphous materials and materials with a nanocrystalline structure are included in this category [7].

1.2 Crystalline Silicon

Crystalline Silicon (c- Si) has a relatively small and indirect band gap of approximately 1.12 eV. Moreover, highly pure c- Si has a small exciton binding energy of (~14) meV [9]. Silicon is the most prevalent semiconductor used in microelectronics and photonics; it is produced in higher volume for lower cost than any other semiconductor. The band gap of silicon leads to efficient detection of visible light and conversion of sunlight into electricity. Easily integrated with other microelectronics, silicon is used in many forms including (crystalline, amorphous, and porous) in numerous optoelectronic devices [10]. Optical quality silicon is highly transparent in the far – infrared region and opaque in the visible and ultraviolet region [7, 11]. Silicon lattice has a diamond-like structure and it consists of two interpenetrating FCC lattice as shown in figure (1.2) [12]. Silicon surface has high absorptivity for oxygen and the growth rate of oxide layer on silicon surface is nearly (2 nm/min) under ambient condition. This oxide layer has a considerable effect on the absorbity of the surface for photons of energies higher than (6eV) [9].

Reducing dimensionality of bulk silicon to nano-scale silicon (PS) leads to appreciable change in optical, electrical and electronic properties [9].

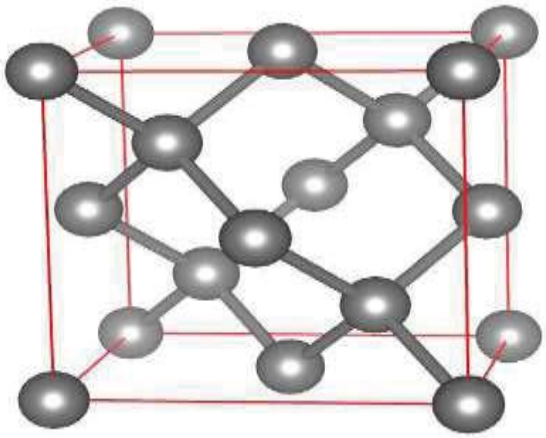

Fig. (1.2): The diamond lattice structure of Si [12].

1.3 Porous Silicon (PSi)

Porous silicon is a solid silicon with voids there in, is one of the most important porous materials with a wide range of applications from batteries and fuel cells to drug delivery and diagnostics [1–3]. Although optoelectronics, especially light emission, has been porous silicon's primary area of interest for the last 25 years, the material has recently found its way to cosmetics, consumer care, nutrition, and food industry, figure (1.3) shows porous silicon membrane on silica support [13]. The preparation of porous silicon is rather simple and inexpensive. It can be performed by several methods depending on the desired structure and properties. It shows highly tunable structural, mechanical, optical, electrical, thermal, emissive, and physiochemical properties. Some of its properties like luminescence and medical biodegradability are direct consequences of nanscale porosiication and are not observed in bulk silicon. The properties of porous silicon structures, like other porous materials, are classified by their dominant pore dimensions. Structures with pore dimensions below 2 nm and above 50 nm are called microporous and macroporous silicon, respectively; those lie between are called mesoporous silicon, as shown in table (1.2). Due to the extremely rich details with respect to the range of variations in pore size, shape, orientation, branching, interconnection, and distribution, morphology is the least quantifiable aspect of this material. Figure (1.4) schematically demonstrates the four different morphological aspects of porous silicon and their variations, and figure (1.5) shows cross-sectional SEM morphology of different porous silicon structures. Various morphologies and different pore dimensions give porous silicon extremely diverse structural, mechanical, optical, electrical, thermal, emissive, physiochemical, and biochemical properties. Table (1.3) compares the properties of mesoporous silicon with those of bulk silicon. As the structure and surface chemistry of porous silicon can be precisely controlled during

properly chosen fabrication process and appropriate post-fabrication treatment, the material's properties can be tuned according to the desired application. Tuning of porous silicon properties can be performed by manipulating its structural parameters, altering its surface chemistry, or impregnating other materials [14].

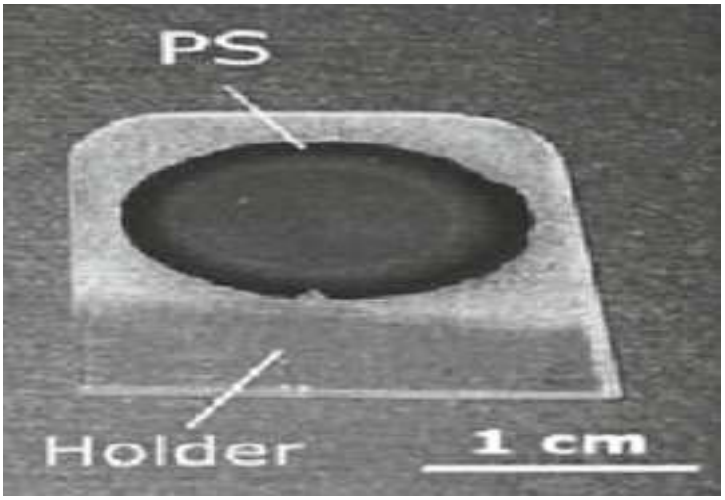

Fig. (1.3): Porous silicon membrane [13].

Table (1.2): The classification of the pore size [15]**.**

Pore Width(nm)	***Type of Pore***
≤ 2	Microporous
2-50	Mesoporous
> 50	Macroporous

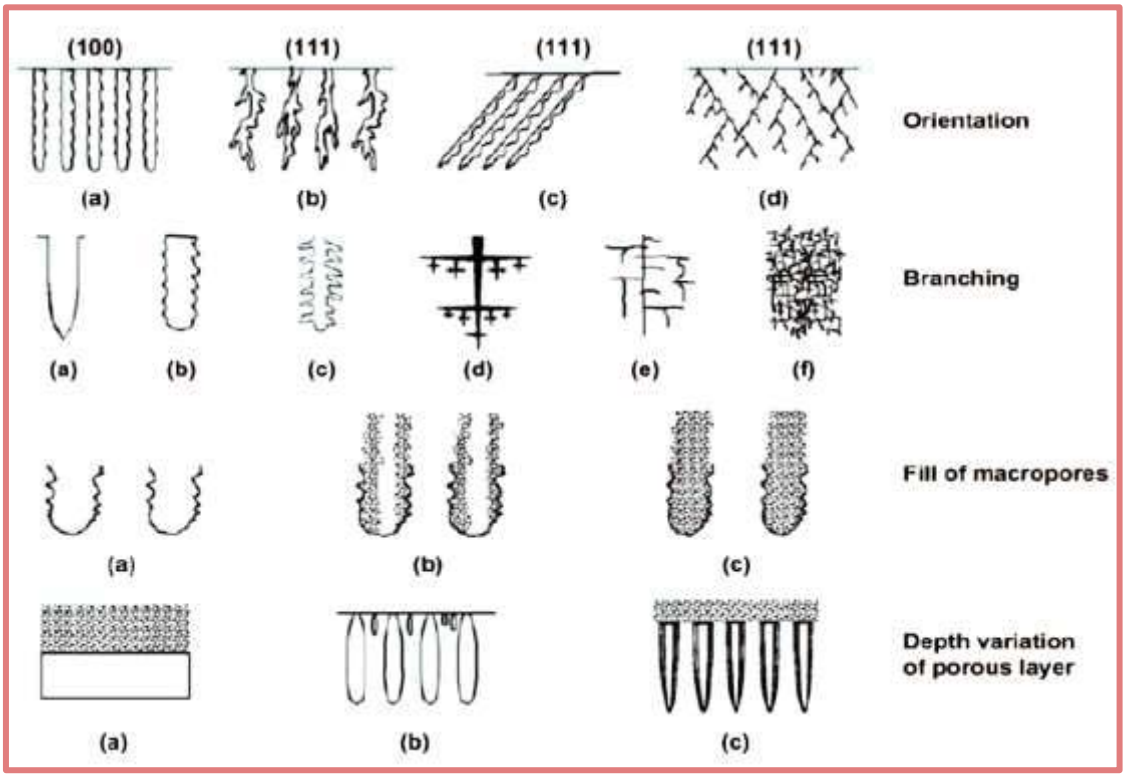

Fig(1.4): Morphological characteristics of porous silicon [16].

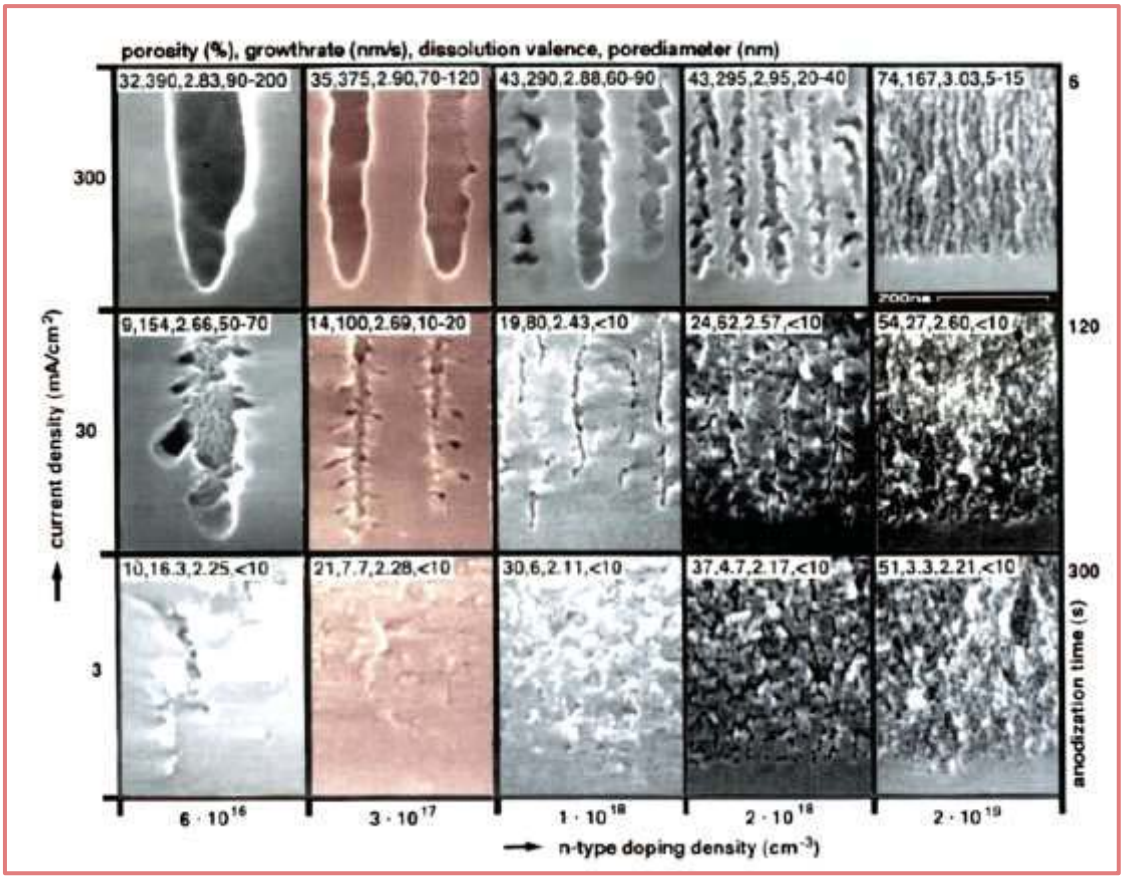

Fig.(1.5): Cross-sectional SEM micrographs of various porous silicon structures formed by (electrochemical etching) [17].

Table (1.3): Tunable properties of mesoporous silicon in comparison with those of bulk silicon [14].

Application	Property	Bulk silicon	Mesoporous silicon
structure	Porosity	-	20-95%
	Density	2.33g/cm^3	0.12-1.9g/cm^3
	Pore size (diameter)	-	2-50nm
	Surface area	-	100-800m^2/g
	Lattice structure	Diamond	Diamond
Mechanical	Young's modulus	160GPa	1-100GPa
	Hardness	11.5GPa	0-2-10GPa(layer)
			0.05-1GPa(composite)
	Yield strength	7GPs	-
	Facture toughness	0.6MPam$^{1/2}$	-
Optical	Band gap	1.1eV	1.1-3.2eV
	Infrared refractive index	3.5	1.1-3
	Color	Gray	All colors(layer)
			Brown-Yellow(particle)
	Reflectivity(500-1000nm)	10-35%	0.1-10%
Electrical	Resistivity	10^{-2}–10^3 Ωcm	10^3-10^{12} Ωcm
	Free electron mobility	1350 cm^2/Vs	0.1-30cm^2/Vs
	Hole mobility	480 cm^2/Vs	2-6cm^2/Vs
	Dielectric constant	11.5	2-8
Thermal	Conductivity	150 W/mK	0.03-20 W/mK
	Melting point	1414ºC	800-1414ºC
	Specific heat	0.7J/gK	-
	Diffusivity	0.8cm^2/s	-
Emissive	PL wavelength	1000-1200nm	400-1300nm
	PL efficiency	10^{-6}	0.01-0.23(films)
			0.01-06(suspensions)
	EL efficiency	10^{-5}	0.01-0.1
Physiochemical	Isoelectric point	pH 1.6-2.5	pH 1.6-7.7
	Zeta potential(pH7)	-(45-70)mV	-
	Surface wettability	5-96º	<0.5-167º
Biochemical	Medical biodegradability	-	Months(implants)
			Hours (nanoparticles)

1.4 Properties of Porous Silicon

1.4.1 Optical Properties of Porous Silicon

Various explanations have been proposed for the strong visible luminescence from porous silicon, the most popular being quantum confinement in nanometer size silicon crystallites. The microstructure and optical properties of PSi have not been determined with enough resolution to confirm the quantum confinement model directly.

Predictions of the quantum confinement model are that the energies of the valance and conduction band edges should be correlated and depend on the size of the Si microstructures. Buuren and Tiedje used X-ray absorption and photoemission to measure the energies of the conduction and valance band edges of PSi relative to bulk Si and compared the results with quantum confinement model [18].

A significant blue shift of the absorption edge and visible room temperature photoluminescence are attributed to the existence of a porous sponge –like silicon skeleton with dimensions of few nanometers. By adjusting the formation conditions, the dimensions of the porous silicon skeleton can be increased several orders of magnitude and its optical properties tuned [19].

Since the first work on -comparing the optical transmission of bulk Si with that of free-standing PSi films by Lehman and Gosele, optical transmission measurement has become one of the most powerful tools for understanding the microstructure and luminescence mechanism of the PSi. Lehman and Gosele attributed the increasing of the transmission below the direct gap to quantum confinement effects. Sagnes et al. have measured the transmission of the free-standing PSi films with porosities in a range of (45%-79%) and absorbed a continuous blue-shift of the transmission curves with an increase in the porosity of the PSi films [20]. Jan believed that the

photo absorption corresponds to the generation of electron -hole pairs, whose energies are much larger than the energy gap of bulk Si as a result of the quantum confinement effect, which the luminescence corresponds to the recombination of electron-hole pairs. The absorption coefficient has been measured in PSi by optical transmission, Photoluminescence Excitation (PLE), and Photothermal Deflection Spectroscopy (PDS) [21].

1.4.2 Electrical Properties of Porous Silicon

The great interest in the PSi material is because this material possesses unusual physical properties, which gives new chances to develop many technological applications.

Within the last decades the PSi structures have been used not only to emit light efficiently, but also be capable of guiding, modeling and detecting light.

Consequently, the studies of electrical and photoelectrical properties of PSi – based devices have taken a large space of scientific publications.

The progress towards silicon optoelectronics and photovoltaic devices using PSi layer requires good understanding of the electrical behavior of PSi layer [22, 23]. Bare PSi is insulating with a resistivity which is five orders of magnitude higher than that of intrinsic Si because PSi is depleted from free carriers.

Free carriers depletion is a consequence of the quantum confinement induced widing of the band gap, which reduce the thermal generation of free carriers, and the trapping of free carrier. Trapping can occur during the preparation of PSi either because the binding energy of dopant impurities is increased or because surface states form. The disordered nature of the PSi skeleton and its local crystalline structure are expected to have strong geometrical effects on the conductivity [24]. Several hypotheses were forwarded to explain the low conductivity of porous silicon, these

hypotheses are based on the existence of depleted layers of charge carriers surrounding the pores and on the existence of quantum-size effect [25].

1.5 Porosity of Porous Silicon

The porosity of the PSi is the most important parameter, which characterizes the porous silicon. Porosity is defined as the fraction of void within the PSi layer [25, 26].

The porosity of silicon substrate strongly depends on the preparation conditions such as wafer type, wafer resistivity, HF concentration, etching time and etching current density. It will be retained that it increases when the density of current increases or when the HF concentration decreases. The accessible porous silicon values typically included between (15% and 90%). It is significant to note that porosity is an average value and that for the same porosity; various material morphologies can be obtained [26].

The porosity can be determined by weight measurements. The porosity of the layer can be determined by weighting the silicon substrate before and after etching process (m_1 & m_2) respectively and again after removing the porous silicon layer by using a molar NaOH (m_3). The porosity is given by the following equation [26]:

$$\boldsymbol{\gamma(\%) = \frac{m_1 - m_2}{m_1 - m_3}} \qquad \textbf{..... (1.1)}$$

Where; γ is the porosity.

According to the above formula, it is necessary to use the thickest samples possible [26].

1.6 Preparation Techniques

1.6.1 The Etching Process

Various etching techniques can be divided into wet and dry categories according to the chemical reaction on the gas-solid and liquid-solid interface [9]. In the wet etching, chemical acid solutions are used to dissolve silicon substrate by chemical reactions [27]. Wet etching of silicon can be achieved in different ways [9, 28]:

- Laser Induced Etching process(LIE)
- Photochemical Etching process (PC)
- Photo electro Chemical Etching process (PEC)
- Stain Etching process
- Electrochemical Etching process

1.6.2 Electrochemical Etching Mechanism

In most cases, PSi structure is formed by electrochemical etching (ECE) of Si wafers in electrolytes including hydrofluoric acid (HF) and surfactants (mainly ethanol). Because the cleaned, polished Si wafer surface is absolute alcohol is added to the electrolyte [29, 30]. It increases the wet ability of the substrate and in turn helps the electrolyte penetrating into the pores, by which laterally homogenous current density can be maintained to result in the formation of uniform PSi layers. During the electrochemical etching of a Si surface, H_2 gas evolves to form tiny bubbles attached to the surface. When ethanol is present in the electrolyte, these bubbles can easily leave the surface because of the decreased surface tension of the liquid. Additionally, the bubbling enhances the liquid circulation in the electrolyzation cell, which helps the transport of reactants and side products, to be able to synthesize uniform layers with high reproducibility, the applied anodic current density and etching time are monitored, controlled and kept at a particular constant level required during the

process. The electrolization cell is made of a highly-acidic resistant polymer such as Teflon. The cathode of the anodization cell is generally made of Platinum or other HF-resistant conductive material, and the Si surface itself is the anode [31]. The backside of the Si wafer is placed on a metal disk and sealed with an O-ring on the front side where the anodization takes place [32]. Figure (1.6) shows the energy band diagram of (n, p) type silicon wafers immersed in HF and distribution of charge near the silicon /HF interface. For electrolytic solutions such as HF, the mixed reduction potential acts as an equivalent Fermi level and is determined by the chemical species within the solution. When a silicon wafer is immersed in an electrolytic solution, transfer of electrons across the interface occurs until the Fermi level of the silicon wafer EF matches the mixed reduction potential E_{Redox} of the electrolytic solution. For n-type silicon in contact with an electrolyte solution such as HF, EF is generally higher than E_{Redox} of the solution. To equilibrate, electrons are transferred from the silicon to the electrolyte, forming a space charge region beneath the silicon surface, which contains a net positive charge that is reflected in upward bending of the band edges, as seen in figure (1.6) a and b. For p-type silicon in contact with HF, the Fermi level is lower than the reduction potential in the solution and electrons flow from the electrolyte into the semiconductor to equilibrate. This results in downward bending of the band edges, as seen in figure (1.6) c and d. Thus, unlike a metal with a fixed work function, E_{Redox} of the HF solution induces depletion in both n-type and p-type silicon [33].

While figure (1.7) shows the reaction mechanism of formation of porous structures on crystalline silicon. The net reaction for silicon etching is given in equation [33]:

$$\mathbf{Si + 6HF + h^+ \rightarrow SiF_6^{-2} + H_2 + 4H^+ + e^-} \quad \text{..... (1.2)}$$

Where h^+ and e^- represent hole and electron respectively.

Hydrogen gas evolution resulting from this reaction can be observed from the silicon surface during the etching process. It is evident from the reaction that silicon atoms are knocked out from the surface generating porous structure containing nanocrystallites of silicon [33].

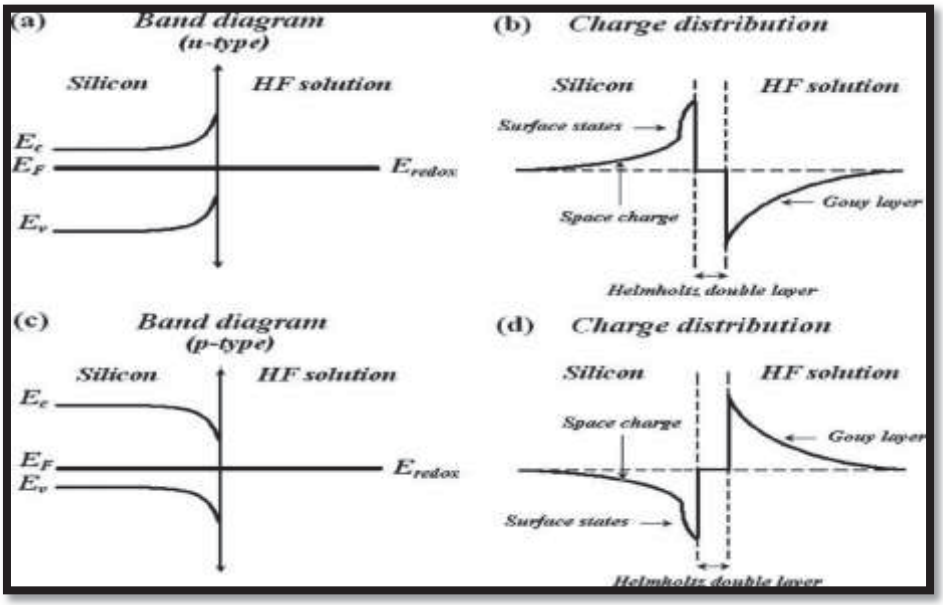

Fig.(1.6) :(a) and **(c):** energy band diagram of an (n and p-type silicon wafers) immersed in HF respectively**: (b)** and **(d):** the distribution of charge near the silicon /HF interface for (n and p-type silicon wafers) respectively [32, 34].

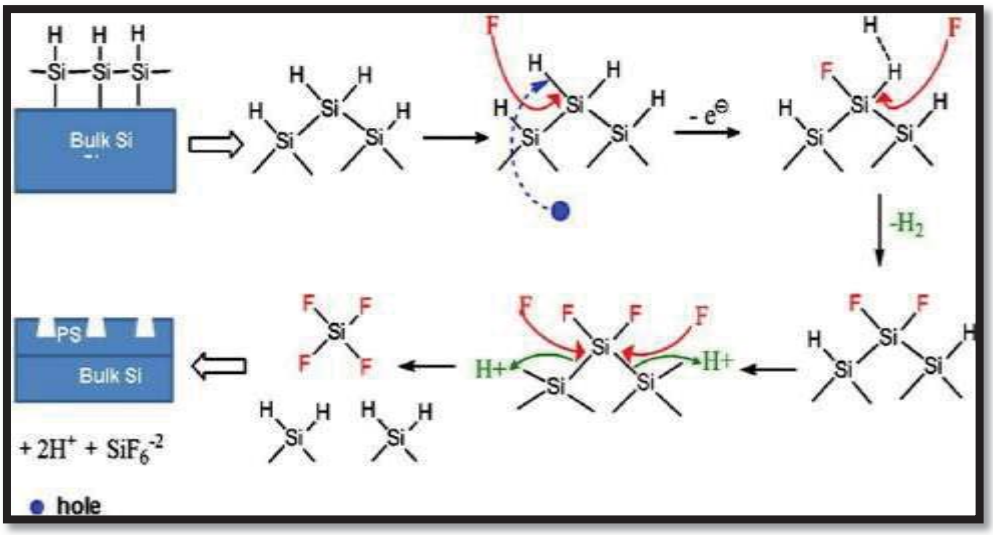

Fig.(1.7): Reaction mechanism of formation of porous structures on crystalline silicon [33].

1.7 Transparent Conducting Oxide (TCO)

Transparent conduction oxides (TCOs) paid a great deal of attention to what is owned by the unique qualities of the material advantage for other materials, such as thin films oxides that possess high optical transmittance in the visible region and a high reflectivity in the infrared region and in improving the performance of the solar cells [35,36]. In modern technology, the creation of the TCOs is done by using metallic oxides and sometimes sulphides. This is because these types of metals have high levels of electrical conductivity. The chemicals used also have high levels of thermal and chemical stability. One of the metals that are used as TCO is Zinc Oxide. Zinc Oxide (ZnO) is a band gap semiconductor which belongs to the II-VI semiconductor group. The n-type class of doping is used in zinc oxide because of the favorable properties. Some of the properties that make Zinc Oxide a good semiconductor include the good transparency, the mobility of the electrons, the wide bandgap and the high room temperatures. According to Andrew, 2004, the properties of the TCOs are dependent on the deviations of the stoichiometric nature and the type of impurities which exist in the host. Energy where it contains a high concentration of free electrons in the conduction band and wide applications of transparent conductivity oxides including [37, 38].

- Solar cell regimes windows and anti-reflective coating.
- Deposition on the windows of the buildings to secure low-lying emissivity glass.
- Sensors into every gas manufacturing.
- The industry of flat screens display of the TV and computer.

1.8 ZnO properties

ZnO crystallizes preferentially in the stable hexagonal wurtzite structure at room temperature and normal atmospheric pressure as shown in figure

(1.8). It has lattice parameters of a= 0.3296 nm and c = 0.520 nm with a density of 5.60 g. cm^{-3}. The electro negativity values of O^{-2} and Zn^{+2} are 3.44 and 1.65, respectively resulting in very strong ionic bonding between Zn^{+2} and O^{-2}. The basic characteristics of ZnO are the polar surfaces that are formed by oppositely charged ions produced by positively charged Zn^{+} (0001) and negatively charged O^{-} (0001) polar surfaces. It is responsible for the spontaneous polarization observed in ZnO. The polar surfaces of ZnO have non-transferable and non-flowable ionic charges [39]. The ZnO is a wide direct band gap (~ 3.3 eV) semiconductor material [39]. The II-VI semiconductor Zinc Oxide (ZnO) has great potential for applications in short-wavelength opto-electronics, light-emitting diodes, lasers and detectors. It also has the potential to compete GaN, due to its promising properties such as a larger exciton binding energy (60 meV), lower cost, and higher chemical etching rate [40, 41], which gives it a high potential for room temperature light emission, more resistant to radiation, and multifunction as it has piezoelectric [42], dielectric, transparent, semiconducting oxide and optoelectronic applications in UV-Blue spectral range [43]. ZnO is a unique material that exhibits both semiconducting and piezoelectric properties. In the past decade, numerous studies have been made on both production and application of one dimensional ZnO compared to other semiconducting materials [43]. In addition, due to its direct band gap and its large photoresponse, ZnO is also very suitable for UV – photo – detector applications [44]. The high cohesive energy of ZnO which is ~ 1.89 eV makes it a highly stable and perhaps most radiation hard material amongst the direct band gap semiconductor family, which ensures a long life and a high degradation threshold of ZnO based optoelectronic devices [45]. The high melting and boiling points of ZnO allow one to explore a variety of heat treatments required for alloying purposes and device formation. Being an oxide, ZnO also enjoys the extreme stability

against the oxidation problem which can severely affect the device performance as in case of some of the III- V and II-V semiconductors such as GaAs, InAs and ZnS etc. [46]. Other advantages of ZnO are the resistance to high energy radiation, which makes it suitable for space applications, as well as the stability and amenability to wet chemical etching , which can be exploited for the fabrication of small size devices [47]. Since the Ultraviolet (UV) Photodetector have a wide range of applications in military and civilian areas, most of the applications are directed toward the environmental monitoring, solar astronomy, and missile warning systems [48, 49]. Wide-band gap materials are under intensive studies to improve the responsivity and stability of UV photodetector [50, 51]. Among them, ZnO is of great interest due to its strong UV photoresponse and is very promising material because of its unique optical and electronic properties. Large band gap semiconductor is of interest in microelectronics and optoelectronics .Thin films of ZnO have been reported to display good conductivity and high transparency in the visible region [52]. Table (1.4) shows a compilation of the basic physical parameter for ZnO.

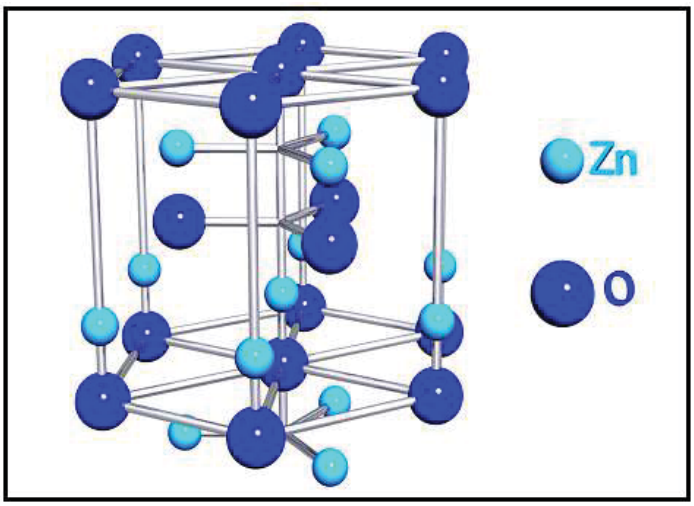

Fig. (1.8): Wurtzite structure of ZnO [53].

Table (1.4): Physical properties of ZnO wurtzite structure [53].

Property	***Value***
Lattice parameters at 300 K (a_o , c_o)	*0.32495nm, 0.52069nm*
c_o/a_o	*1.602 (ideal hexagonal structure shows 1.633)*
Density	*5.606 g .cm^{-3}*
Melting point	*1975 ˚C*
Thermal conductivity	*0.6 W. cm^{-1} . ˚C^{-1}*
Refractive index	*2.029*
Energy gap	*3.37 eV , direct*
Breakdown voltage	*$5x10^6$ V cm^{-1}*
Saturation velocity	*3x 10^7 $cm.s^{-1}$*
Exciton binding energy	*60 meV*
Electron effective mass	*0.24 gm*
Hole effective mass	*0.59 gm*
Ionicity	*62 %*
Dielectric constant	*7.6*
Heat capacity C_p	*9.6 cal / mol K*
Young's modulus E(bulk ZnO)	*111.2 ± 4.7 G Pa*

1.9 Li_2O properties

Lithium oxide (Li_2O) or lithia is an inorganic chemical compound. It is a white solid. Although not specifically important, many materials are assessed on the basis of their Li_2O content as shown in figure (1.9). For example, the Li_2O content of the principal lithium mineral spodumene ($LiAlSi_2O_6$) is 8.03% [54, 55]. In the solid state lithium oxide adopts an antifluorite structure which is related to the CaF_2 fluorite structure with Li cations substituted for fluoride anions and oxide anions substituted for

calcium cations [56]. The ground state gas phase Li_2O molecule is linear with a bond length consistent with strong ionic bonding [57, 58]. VSEPR theory would predict a bent shape similar to H_2O. Table (1.5) shows a compilation of the basic physical parameter for Li_2O.

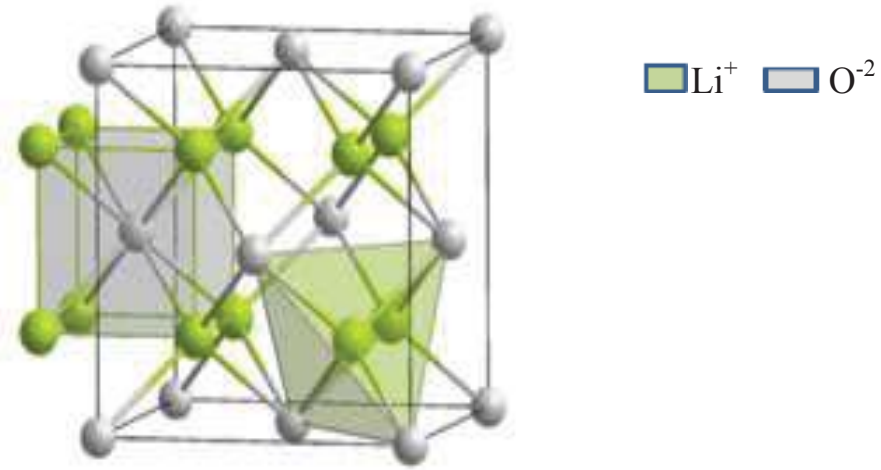

Fig. (1.9): structure of Li_2O crystal.

Table (1.5): Physical properties of Li_2O Cubic structure [59].

Property	***Value***
Chemical formula	*Li_2O*
Molar mass	*29.88 g/mol*
Appearance	*white solid*
Density	*2.013 g/cm^3*
Melting point	*1438 °C*
Boiling point	*2600 °C*
Solubility in water	*reacts violently to form LiOH*
log P	*9.23*
Refractive index (n_D)	*1.644*
Crystal structure	*Antifluorite (cubic), cF12*
Heat capacity (C)	*1.8105 J/g K or 54.1 J/mol K*

1.10 A brief Summary of Thin Films

The term thin films is usually called for a layer or several layers of certain atoms whose thickness may not exceed one micrometer produced by the intensification of atoms or molecules that have unique important characteristics that vary from whether they are a thick particle such as physical and engineering properties [60]. The thickness of these thin films and the ease of cracking when deposited on other substances used as bases of sedimentation depends on the type of base as silicon, quartz, glass, and FTO and the nature of use [61]. It is used in the manufacture of electronic devices in the form of electro-optical, transistors, capacitors, resistors, and optoelectronics devices [62].

1.11 Thin films preparation methods

There are various technology methods for preparing thin solid films for research, development and production purposes. The wide and important applications in thin films field motivate researchers to introduce different methods to prepare the films, according to the scientific progress. The method of preparing thin films also revaluated and became on a high degree of accuracy in specifying the thickness and homogeneity of film. Some of these methods are suitable to a certain materials and not suitable for others, some of them are simple and the others are complicated. Generally, the preparing method depends on many factors such as the materials used. The field of using thin films can be divided into two principal kinds, physical and chemical methods which are shown in figure (1.10) [63].

Figure (1.11) illustrates the three major steps during this process, namely nucleation, crystal growth and film formation. At the same time, these processes allow atoms or molecules to relocate at positions with lower free energy [64].

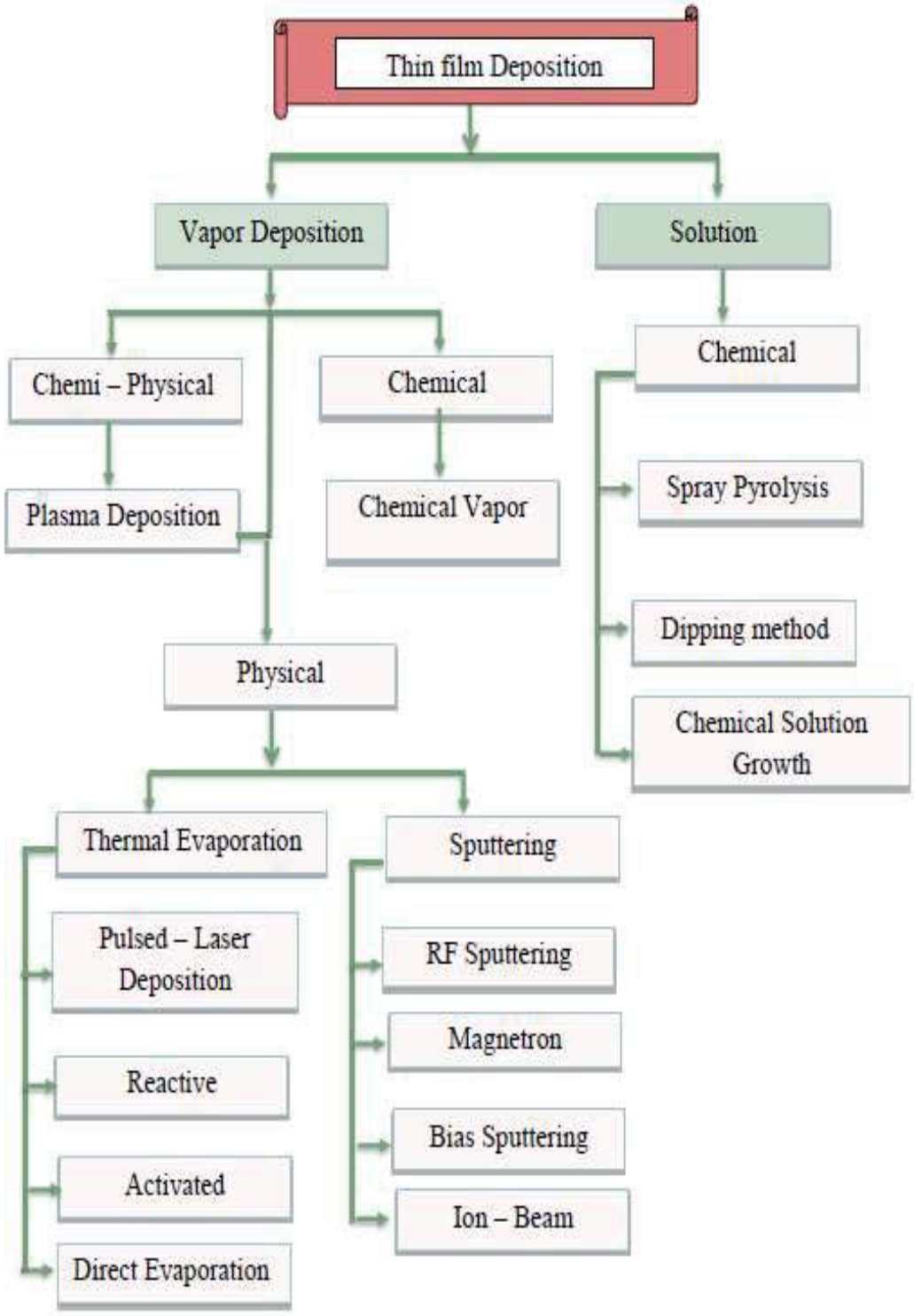

Fig.(1.10): Classification of thin film deposition techniques [63].

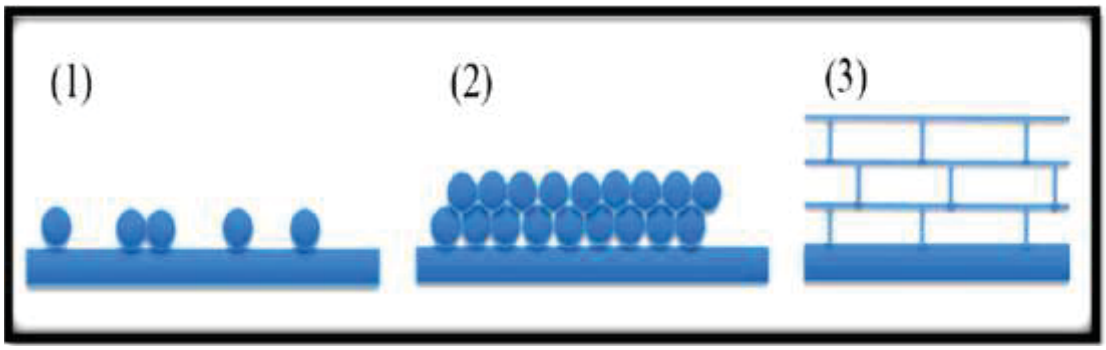

Fig.(1.11): An illustration of the process of:**(1):** nucleation **(2):** crystal growth and **(3):** film formation [64].

1.12 Chemical Precipitation Method

Chemical Precipitation is the process of conversion of a chemical substance into a solid from a solution by converting the substance into an insoluble form or a super-saturated solution [65]. When the reaction occurs in a liquid solution, the solid formed is called the precipitate. The chemical agent that causes the solid to form is called the precipitant.

Without sufficient force of gravity (settling) to bring the solid particles together, the precipitate remains in suspension, as shown in figure (1.12). After precipitation, especially when using a centrifuge to press it into a compact mass, the precipitate may be referred to as a 'pellet'. Precipitation can be used as a medium. The precipitate-free liquid remaining above the solid is called the 'supernate' or 'supernatant'. Powders derived from precipitation have also historically been known as 'flowers'. When the solid appears in the form of cellulose fibers which have been through chemical processing, the process is often referred to as regeneration.

Chemical precipitation method is recently gaining momentum for the fabrication of electrolyte materials for solid oxide fuel cells (SOFCs) due to its cost-effectiveness, high yield, and simplicity of the process requirements.

Chemical precipitation has the following advantages [66]:

1. Simple, low-cost pre-treatment technology.
2. Precipitation methods reduce the time required to settle suspended solids.
3. Permanent.
4. Immediate results.
5. Efficient.
6. Easily implemented.
7. Easy to monitor.
8. Chemical precipitation offers many advantages as a treatment.

Chemical precipitation (Hydroxide precipitation) is most used commonly in industry and produces a high-quality effluent when applied. Often, coprecipitaion of a mixture of metal ions will result in residual metal solubilities lower than those that could be achieved by precipitating each metal at its optimum pH. Some common limitations of the hydroxide process are as follows [67]:

1. The theoretical minimum solubility for different metals occurs at different pH values. For a mixture of metal ions, it must be determined whether a single pH can produce sufficiently low solubilities for the metal ions present in the water.
2. Hydroxide precipitates tend to resolubilize if the solution pH is increased or decreased from the minimum solubility point; thus, maximum removal efficiency will not be achieved unless the pH is controlled within a narrow range.
3. The presence of complexing ions, such as phosphates, tartrates, ethylenediaminetetraacetic acid (EDTA), and ammonia may have

adverse effects on metal removal efficiencies when hydroxide precipitation is used.

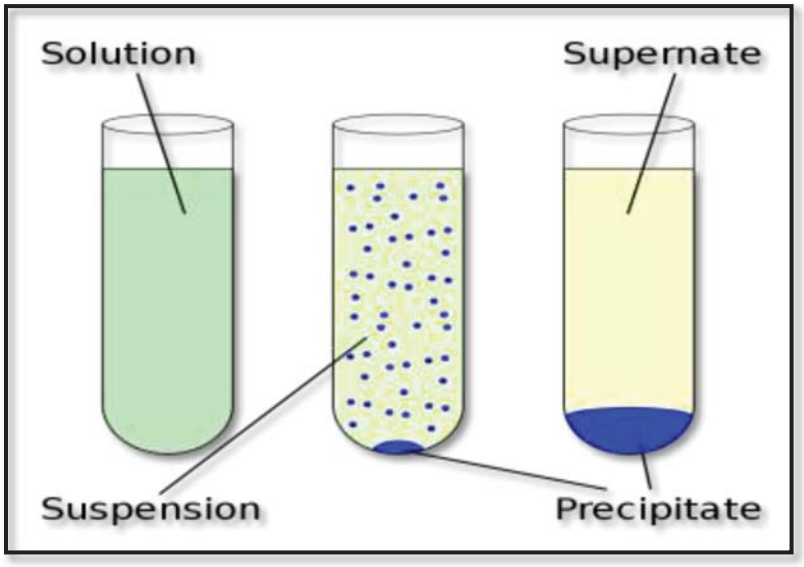

Fig.(1.12): Chemical Precipitation Method [67].

1.13 Simple precipitation method

It is a type of chemical reaction which is defined as breaking the internal chemical bonds in the reactants and rearranging them in order to form new chemical bonds in the materials resulting from the chemical reaction, which results in new materials that differ in chemical and physical characteristics [67].

1.14 Literature Review

The literature survey in the field of interest can be summarized as follows:

In (2011), Wei et al. reported three kinds of heterostructures composed of n-type zinc oxide (ZnO) film or nanowires or nanotubes covered with a p-type cuprous oxide (Cu_2O) thin film respectively fabricated with a simple and low-cost electrochemical deposition method. Structural, optical, and

electrical studies identified the formation of the three kinds of proposed Cu_2O/ZnO p–n heterojunctions. Photovoltaic properties measurements demonstrated that the Cu_2O/ZnO film/nanowire based solar cell exhibited an obviously enhanced performance in comparison with the corresponding planar film solar cell due to the increased p–n junction area and improved charge carrier collection ability by using ZnO nanostructures. As a result, the Cu_2O/ZnO film/nanotube solar cell had a maximum short-circuit current density under the same conditions. But, the open-circuit voltage and conversion efficiency decreased a little as the formation of ZnO nanotubes through chemical etching caused short circuits between the Cu_2O layer and the conductive glass substrate. This study demonstrates that the proposed strategy to improve the solar cell performance realized by electrochemical deposition has potential in producing cheap and environmentally friendly solar cells [37].

In (2011), Kou et al. have studied nanosheets of ZnO on porous Si (PS) at different applied potentials by electrodeposition approach. Thus, ZnO grown on PS could be used as photoelectric materials due to its larger photoelectric effect compared to Si wafer according to open-circuit potential (OCP) study. Optical band gap measurements were made on samples using UV–visible spectrophotometer thus giving a band gap of 3.35eV [67].

In (2011), Isa et al. have been prepared PS was by chemical etching of p-type silicon wafer where the etchant consists of mixture of hydrofluoric acid (HF) and nitric acid (HNO_3). The PS was characterized by Scanning Electron Microscope (SEM) and Photoluminescence Spectrometer. The porosity of the PS was in the range of (49-80) % and it is dependent on etching time. The peak of the PL ranges from 636 nm to 640 nm and the intensity of PL increase proportionally with the etching time. Band gap

energy of PS was higher than silicon (1.11 eV) which is from 1.93 eV to 1.95 eV and the blue shift of the PL peak was observed as the porosity increases [68].

In (2012), Suhail et al. reported that the conversion efficiency of Si solar cell of 500^{+}m thickness was improved by etching the front solar surface using the photochemical etching technique. The etched surface was coated by a nanolayer of CdS nanoparticles of (4-8)nm dimension. The CdS nanolayer was passivated with polyamide nylon. This treatment highly improved the response of the solar cell and increases its efficiency from (7.8 to 14.8)%. The explanation of the improvement was referred by the light trapping in the silicon nanospike layer, and due to the efficient conversion of the UV to the visible light by CdS nanoparticles. The matching index of the coated surface with the silicon solar cell helps in the improvement of the total efficiency of the silicon solar cell [69].

In (2012), Shatkovskis et al. have been reported that silicon solar cells were produced by p-type, crystalline silicon wafer. The manufactured solar cells were of 450 μm total thickness, the junction depth was of (0.5–0.7) μm. Porous silicon technologies were adapted to enhance cell efficiency. The production of porous silicon layer was carried out in HF: ethanol = 1:2 volume ratio electrolytes, illuminating by 50 W halogen lamps at the time of processing. The etching current was computer-controlled in the limits of (6–14) mA/cm^2, etching time was set in the interval of (10–20)s. The characteristics and performance of the solar cells samples were carried out by using Xenon 5000 K lamp light. Current-voltage characteristic studies have shown that porous silicon structures formed influence the degree of dark and lighting parameters of the samples. Exactly it influences serial resistance of the cells. It has demonstrated, the formation of porous silicon structure induces an increase in the electric

power produced of solar cell. Conversion efficiency increases also respectively to the initial efficiency of cell. Increase of solar cell maximum power in 15 or even more percent is found. The highest increases in power have been observed in the spectral range of $\Delta\lambda \cong$ (450–850) nm, where ~60 % of the 1.5 A spectra solar energy is located. It has been demonstrated that porous silicon technology is effective tool to improve the silicon solar cells performance [70].

In (2013), Hadi et al. reported that the porous silicon (PS) has been fabricated by Photo-electrochemical etching. Porous silicon was anodized on n-typeSi in light using a current density of 20 mA/cm^2 for 10 min. The porous structure formation was confirmed using XRD and AFM studies. The root mean square (RMS) roughness of the Porous silicon layer is found to be around 47.5 nm and the ten point height was 317 nm. The average of pores diameter was 419.98nm, and the grain growth is columnar with a (211) preferred orientation. The grain size of the PS was estimated from the Scherer's formula and found to be 73 nm. All the properties of the porous silicon layer, such as porosity and the thickness depend on the anodization parameters. The porosity (P) was approximately 77%. The thickness of the layer formed during an anodization in constant current was 3.54 nm in gravimetric method, while its value was 1.77 nm by using the theoretical relation [71].

In (2013), Nayef et al. reported that porous silicon layers from p-type silicon was prepared by electrochemical etching method . And was studied the morphology properties of PS samples by changing etching time and imaged PS sample in Atomic force microscopy(AFM). The found that from AFM images show the PS layer has sponge like structure, and average diameter of pore and thickness of PS layer decreasing with silicon <111> oriented more than with silicon <100>.

And also found that when increasing etching of time porosity of PS increasing specifically in <100> [72].

In (2014), Keramatnejad et al. reported the effect of porous silicon substrates with various structures on response in ultraviolet range of a zinc oxide nanowire based heterojunction ultraviolet detectors. This was realized through modifications made in band gap of silicon as a result of porosification for the purpose of increasing the sensitivity and selectivity. Different porous substrates were prepared by electrochemical anodic etching process at different anodization times, current densities and acid concentration which is considered an easy and cost-effective fabrication process that makes the proposed heterojunction a suitable choice for ultraviolet sensing applications. The electrical and optical properties of the prepared samples were measured and the sample with highest porosity exhibits the most selective response with the highest sensitivity (2×10^4 at −3.4V) and the lowest dark current (1.2×10^{-8} A at -3.4V) among all samples, although the sample with crystalline silicon substrate shows the highest responsivity (1,109A/W at 356 nm)[73].

In (2015), Abd et al. reported that the porous silicon (PSi) nanocrystalline was prepared by Photoelectrochemical etching (PECE). PSi was characterized by the measurement of X-ray diffraction (XRD), Fourier transform infrared spectrophotometer (FTIR) and atomic force microscopy (AFM). The FTIR analyses indicate that Si dangling bonds of the as-prepared PSi layer has large amount of hydrogen, forming a weak Si–H bonds. The structural, morphological, optical, and electrical properties of CuO NPs have been studied. X-ray diffraction measurement confirms that the CuO NPs were tetragonal crystal structure. AFM reveals that produced CuO NPs have a spherical shape. The energy band gap of CuO NPs

prepared was found to be about (2.61eV). The effect of CuO NPs diffused on Psi heterodiode was reported [74].

In (2015), Habubi et al. reported the effect of embedding colloidal cadmium selenide nanoparticles on the characteristics of porous silicon Al/ porous Si//p-Si photo detectors prepared with 7 mA/Cm^2 electrochemical etching for 15 min. the spherical cadmium selenide nanoparticles of size 35- 60 nm, synthesized by laser ablation in methanol, had covered the pore walls of porous silicon matrix. Structural, morphological and optical properties of porous silicon and cadmium selenide nanoparticles were characterized by x-ray diffraction, photo-luminescence, transformation infrared spectroscopy, scanning electron microscopy, transmission electron microscopy, atomic force microscopy and UV-Vis spectrophotometer. Electrical and photosensivity of porous silicon photodetectors have been investigated before and after the embedding of cadmium selenide nanoparticles. The ideality factor of porous silicon has decreased after the incorporation of cadmium selenide nanoparticles in porous silicon. Photodetector sensitivity has increased from 0.5 to o.8 A/W at 800 nm after embedding CdSe NPs in silicon pores [75].

In (2016), **Abdulridha et al.** reported that the SnS thin film were prepared by thermal evaporation technique on porous silicon layer which prepared by anodization technique at 32 mA/cm^2 etching current density and etching time 15min.The characteristics of porous silicon and SnS were investigated by using x-ray diffraction XRD, atomic force microscopy AFM, Fourier transformation infrared spectroscopy FT-IR. Dark and illuminated current-voltage I-V characteristics, spectral responsivity, specific detectivity of Al/SnS/PS/n-Si/Al photodiode were investigated after depositing. The spectral responsivity R(λ)of Al/SnS/PS/n-Si/Al photodetectors is around 0.7A/W at 750 nm wavelength and around 0.3 A/W at 400 nm wavelength,

proving that deposition of SnS on porous silicon (PS) photodetectors enhanced the properties porous photodetectors [76].

In (2017), **Mishjil et al.** reported that the ZnO NPs were prepared from colloidal ZnO nanoparticles by using chemical method. The structural, morphological and optical of ZnO thin film have been studied. XRD anaylsis assure that the ZnO thin films were of wurtzite hexagonal crystal structure. AFM investigations showed that the produced ZnO particles have ball-shape with good disposability. The optical energy band gap of ZnO thin film has been determined from optical properties and found to be in the range (3.2 eV). Al/ZnO/Si/Al photodetector heterojunction have two peaks of response located at 415 nm and 780 nm with max sensitivity of 0.6 A/W [77].

In (2017), Shin et al. reported that the PSi Schottky-type heterojunction solar cells by employing graphene transparent conductive electrodes doped with silver nanowires (Ag NWs). The PSi was formed based on metal-assisted chemical etching process, and its porosity was controlled by varying the deposition time of Ag nanoparticles used for the etching. The Ag NWs-doped graphene/PSi solar cells show a maximum power-conversion efficiency (PCE) of 4.03% at deposition time¼ 3s/concentration of Ag NWs ¼ 0.1 (wt%). As deposition time increases, the diode ideality factor and the light absorption increase. As concentration increases, the work function (thus the open circuit voltage) and the transmittance decrease whilst the light absorption increases/the sheet resistance decreases. These trade-offs explain why the PCE is maximized at deposition time ¼ 3 s/concentration ¼ 0.1 wt% [78].

In (2018), Jawad et al. reported that prepared Zinc Oxide (ZnO) thin film by simple chemical method. The structural , topographical and the optical properties of the synthesized thin film were studied by using X- Ray

Diffraction (XRD), Atomic Force Microscopy (AFM), Fourier-Transform Infrared Spectroscopy (FTIR), UV-Vis absorption and Optical microscope (OP) image. The XRD pattern of ZnO thin film deposited on a substrate of glass shows polycrystalline structure, the wurtzite structure with average crystallite size 36.207 nm was appeared. While 3D AFM image show 42.35 nm average grain size with 2.69 and 3.19 nm for each roughness average and root mean square, respectively. PL spectra of ZnO thin film reveals that the emission wavelength of ZnO thin film equal to 400 nm and emission energy of the film (3.1 eV)[79].

In (2018), Ali et al. reported that porous silicon (n-PS) films can be prepared by photoelectochemical etching (PECE) Silicon chips n-types with 15 (mA /cm^2), in 15 minutes etching time on the fabrication nano-sized pore arrangement. By using X-ray diffraction measurement and atomic force microscopy characteristics (AFM), PS was investigated. It was also evaluated the crystallites size from (XRD) for the PS nanoscale. The structural, optical and morphology of TiO_2 NPs has been studied. Analysis (XRD) showed that the structure of (TiO_2) NPs is Tetragonal. While with AFM measurements, it has been realized that the synthesized TiO_2 particles are spherical with an average particle size in the (82 nm) range. It has been determined that the energy band gap of TiO_2 NPs from optical properties and set to be in (5eV) range. It was reported the effectiveness of TiO_2 NPs expansion on the PS Photodetector properties which exposes the benefits in (Al/PS/Si/Al). The built-in tension values depend on the etching time current density and laser flounce. Al/TiO_2/PS/Si/Al photo-detector heterojunction have two response peaks that are situated at 350 nm and (700 -800nm) with max sensitivity ≈ 0.7 A/W. The maximum given detectivity is 9.38 at ≈ 780 nm wavelength [80].

In (2018), Dawood et al. reported that the silver oxide was prepared by high vacuum thermal evaporation at 300 ºC and was deposited on porous silicon. The n-PSi layers were fabricated using electrochemical etching of silicon at a current density of 10 mA/cm^{2}and at 15 min etching time. Surface morphology and electrical properties of this structure have been studied. The X-ray diffraction (XRD) analysis revealed that the peaks at the (220) and (111) planes were dominated for the crystal quality of the AgO films. The band gap of the AgO films was found to be 2.2 eV and 3.2 eV. The positive sign of Hall Effect confirms that the film was of p-type conductivity. The average grain size of pore was measured from the atomic force microscope (AFM) analysis and found to be around 32 nm. The responsively photo detector after deposited AgO for p-AgO/PSi/n-Si heterojunction have revealed increasing in response [81].

In (2018), Agool et al. have been reported that the porous silicon (PSi) was manufactured by using of electrochemical etching method. CdTe nanoparticles (NPs) have been prepared by utilizing the pulsed laser ablation in liquid. The measurements of tunneling microscopy, X-ray diffraction (XRD), Fourier transformation infrared spectroscopy (FTIR) and atomic force microscopy (AFM) were carried out and revealed that the PSi was nanostructured and the produced CdTe NPs were ball shaped. The effect deposited of CdTe NPs on the properties of Psi solar cells assures that there was an improvement upon their properties. The relationship between $1=C^2$ and the reverse bias voltage was observed to be linear. Values of the built in potential were observed to be dependent on the laser flounce, current density and the etching time [82].

In (2019), Wang et al. reported that the porous silicon with high surface area was prepared by using a high yielding and simple reaction in which commercial magnesium powder readily reacts with $HSiCl_3$ with the help of

an amine catalyst under mild conditions. The obtained porous silicon was coated with a nitrogen-doped carbon layer and used as the anode for lithium-ion batteries. The porous Si-carbon nanocomposites exhibited excellent cycling performance with a retained discharge capacity of 1300 $mA\,h\,g^{-1}$ after 200 cycles at 1 $A\,g^{-1}$ and a discharge capacity of 750 $mA\,h\,g^{-1}$ at a current density of 2 $A\,g^{-1}$ after 250 cycles. Remarkably, the Coulombic efficiency was maintained at nearly 100 % throughout the measurements [83].

In (2020), Al Hussan et al. reported that the porous silicon (PSi) was manufactured by using of electrochemical etching method at (10 $mA.cm^{-2}$) current density and 10 minutes etching time. The porous silicone layer was investigated by XRD, AFM and FTIR, and then Li_2O nanoparticles (NPs) were prepared by a simple chemical method. And freshly embedding three drops of (Li_2O) solution using the drop casting technique on the 40^oC porous silicon (n-Psi) method to produce the heterojunction Al /Li_2O/ PSi / Al. The results of current-voltage (I-V) test showed that the solar cell 's maximum power conversion efficiency (PCE) was 2.49% and thus the fill factor was 66.12%. A diffusion of Li_2O NPs on PSi solar cell characteristics assures an improvement on their properties [84].

1.15 Aims of the Work

Aim of this work can be summarized in the following points:

1. Preparation and characteristics study of ZnO and Li_2O nanoparticles (NPs) by (chemical precipitation and simple precipitation) methods, respectively, under different calcination temperatures.
2. Study the Morphological, Structural and Chemical of Porous Silicon (PSi) Produced by Electrochemical etching.
3. Enhancement of solar cell efficiency by Study of the mixing effect for (ZnO:Li_2O) nanoparticles/ porous Si heterojunction solar cell.

And fabrication a device of (n and p- type) heterojunctions [(ZnO/PSi), (Li_2O/PSi)], ((ZnO:Li_2O)/PSi) and multi-junction [(FTO/ZnO/Li_2O/PSi),(FTO/Li_2O/ZnO/PSi),(FTO/(ZnO:Li_2O)/PSi)], and studying of the electrical properties of the heterojunction which include (current-voltage) characteristics under dark and illumination, Photo detector properties.